frontiers in Materials

ORIGINAL RESEARCH
published: 30 April 2019
doi: 10.3389/fmats.2019.00070

Improving Hydrogen Sensing Performance of TiO_2 Nanotube Arrays by ZnO Modification

*Aihua Yu, Haitao Xun and Jianxin Yi**

State Key Laboratory of Fire Science, Department of Safety Science and Engineering, University of Science and Technology of China, Hefei, China

In this work, anodization was utilized to synthesize highly ordered TiO_2 nanotube arrays, and ZnO was successfully decorated onto the surface of as-prepared TiO_2 nanotubes *via* a facile impregnation method. The gas sensing performance of a TiO_2@ZnO composite was systematically studied. At a working temperature of 300°C, the response of TiO_2@ZnO to 100 ppm H_2 was ~340, 2.7 times larger than that of pristine TiO_2. A power–law relationship between the response and H_2 concentration was observed. In addition, the response time was significantly reduced by four times, and improved selectivity to H_2 was achieved. The highly improved sensing performance of TiO_2 nanotubes by ZnO decoration may be attributed to the enhanced oxygen adsorption and formation of n-n heterojunctions.

Keywords: hydrogen sensor, semiconductor, TiO_2 nanotubes, heterojunction, anodic oxidation

OPEN ACCESS

Edited by:
Xiaogan Li,
Dalian University of Technology (DUT), China

Reviewed by:
Han Jin,
Ningbo University, China
Alexander Gaskov,
Lomonosov Moscow State University, Russia

****Correspondence:***
Jianxin Yi
yjx@ustc.edu.cn

Specialty section:
This article was submitted to Functional Ceramics, a section of the journal Frontiers in Materials

Received: *28 January 2019*
Accepted: *01 April 2019*
Published: *30 April 2019*

Citation:
Yu A, Xun H and Yi J (2019) Improving Hydrogen Sensing Performance of TiO_2 Nanotube Arrays by ZnO Modification. Front. Mater. 6:70. doi: 10.3389/fmats.2019.00070

INTRODUCTION

Hydrogen is widely used as an important energy carrier and chemical material. Rapid and accurate detection of hydrogen is highly important due to its risky properties such as low minimum ignition energy (0.017 mJ) and high heat of combustion (142 kJ/g H_2) (Silva et al., 2012). Among the various types of hydrogen sensing technology (Hübert et al., 2011), the resistance-based semiconductor gas sensor has attracted considerable attention due to its high sensitivity, short response time, and long-term stability. On the one hand, using various nanostructures of large surface area, such as nanofibers, nanowires, and nanotubes, has been well demonstrated to favor high gas sensing performance (Li et al., 2015a; Zhang et al., 2016; Chen and Yi, 2018). On the other hand, modification of the materials' surface with noble metals and/or oxides is another simple method to improve the gas sensor performance (Miller et al., 2014).

Among various n-type semiconductors, TiO_2 has been widely studied for gas sensing (Zhao et al., 2015; Wang et al., 2017). A TiO_2 ordered nanotube was proved to have exceptionally high response to hydrogen owing to its unique hierarchical morphology (Varghese et al., 2003). Further improvement of its gas sensing performance was mainly achieved through (1) optimizing the microstructural parameters of the nanotubes such as pore diameter and tube length (Mor et al., 2006) and (2) decorating the surface with noble metals such as Pt and Pd as a catalyst (Joo et al., 2010; Şennik et al., 2010; Xiong et al., 2016). Recently, it was found that by decorating the TiO_2

ordered nanotubes with nanoparticles of non-noble metal, i.e., SnO_2, both the sensitivity and response/recovery speed can be significantly enhanced (Xun et al., 2018), which was ascribed to formation of heterojunctions. Similar heterojunction formation and its promoting effect may also occur when other gas sensing semiconductor oxides are employed as a modifier for TiO_2, which is yet to be studied.

This work synthesized highly aligned TiO_2 nanotubes by anodic oxidation and decorated the nanotubes with ZnO nanoparticles *via* an immersion–calcination method. The sensing performance of the nanotubes was systemically studied, and possible sensing mechanism was discussed.

EXPERIMENTAL SECTION

Synthesis

Chemical reagents were purchased from Sinopharm Chemical Reagent Co., Ltd, China. Ti foils were purchased from Tianjin Ida. Pretreatment of high-purity titanium foils (25-mm thickness, 10 × 20 mm) including cleaning and chemical polishing is similar to that of previous research. The anodization process of the Ti foil was conducted in a two-electrode configuration connected to the DC power supply (Querli, Shanghai) with a voltage of 30 V for 3 h, using electrolyte of ethylene glycol containing 0.3 wt% NF_4F and 5 vol% DI water. The anodized titanium foil was cleaned with ethylene glycol and deionized water in sequence before it was annealed in ambient air at 450°C for 3 h to induce crystallization. For the preparation of TiO_2@ZnO, 0.0652 g of zinc acetate [$Zn(CH_3COO)_2{\cdot}2H_2O$] was dissolved in 20 mL of ethanol as precursor. TiO_2 nanotubes were immersed into the solution for 12 h before they were calcined at 450°C. Two similar samples were prepared for either composition, denoted as TiO_2 and TiO_2-2 for pristine TiO_2 and as TiO_2@ZnO and TiO_2@ZnO-2 for TiO_2@ZnO.

Sensor Test

The typical gas sensor fabrication process and measurement setup parameters can be found in other work (Xun et al., 2018). In brief, the sensor was attached to two electrodes using conductive paste (DAD-87, Shanghai Research Institute of Synthetic Resins) and placed in a testing apparatus with a ceramic heating plate. The temperature and gas-flow rate were controlled by a DC power supply and mass flow controller (CS200, Sevenstar Electronics, Beijing), respectively. Resistance variation was recorded by Keithley 6482. Sensor response was defined as $S = R_a/R_g$ (or R_g/R_a in the case of NO_2 as target gas), where R_a and R_g are the resistance of the sensor in air and test gas, respectively. The response (recovery) time was the time that the resistance variation reached 90% of the total value after introduction (removal) of the target gas.

Characterization

Crystal structure was analyzed by powder X-ray diffraction (XRD, TTR III) using Cu Kα radiation. The morphologies and microstructure of the nanotubes were investigated by scanning electron microscopy (FE-SEM, SU8220) equipped with an energy-dispersive spectrometer (EDS) and transmission electron microscopy (TEM, JEM-2011). X-ray photoelectron spectroscopy (XPS) was performed on an ESCLAB 250 spectrometer using Al Kα as an excitation source and C1s binding energy at 284.8 eV as energy reference.

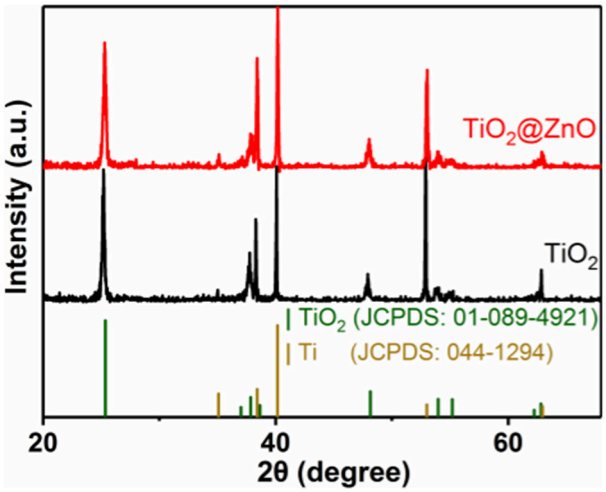

FIGURE 1 | X-ray diffraction (XRD) patterns of pristine TiO_2 and TiO_2@ZnO composites.

RESULTS AND DISCUSSIONS

Material Analysis

Figure 1 shows the XRD patterns of the as-prepared samples. For the pristine TiO_2 sample, all the peaks can be indexed to the anatase structure of titanium dioxide (JCPDS 01-089-4921) and Ti (JCPDS 044-1294). The XRD pattern of the as-synthesized TiO_2@ZnO sample was similar to that of the pristine sample. The diffraction peak of zinc oxide was not observed, which may be due to the low loading amount of zinc oxide.

To illustrate the composition and chemical states of the elements in the samples, XPS studies were carried out, and results were presented in **Figure 2**. Ti and O were present in all the samples, and Zn was detected for the impregnated one (**Figure 2A**). No impurity element other than carbon contamination was observed. As shown in **Figure 2B**, two peaks at a binding energy of ∼458.8 and ∼464.6 eV could be attributed to Ti $2p_{1/2}$ and Ti $2p_{3/2}$, respectively, indicating that the Ti element was present in the form of Ti^{4+}. The binding energy for both Ti $2p_{1/2}$ and Ti $2p_{3/2}$ remained almost invariant after ZnO decoration. **Figure 2C** demonstrates two peaks at a binding energy of ∼1,045.3 and ∼1,022.2 eV, corresponding to Zn $2p_{1/2}$ and Zn $2p_{3/2}$, respectively, implying the +2 oxidation state of Zn in the composite. Besides, the Zn/(Ti + Zn) ratio at the surface of the TiO_2 nanotube was confirmed to be 25.2 at% by XPS analysis. The O 1s peak for both samples can be deconvoluted into two peaks at a binding energy of ∼529.9 and ∼531.4 eV, which corresponded to lattice oxygen (O_{lat}) and absorbed oxygen (O_{abs}), respectively. The $O_{abs}/(O_{abs} + O_{lat})$ ratio of TiO_2@ZnO composites (22.0%) was distinctly larger than that of pristine

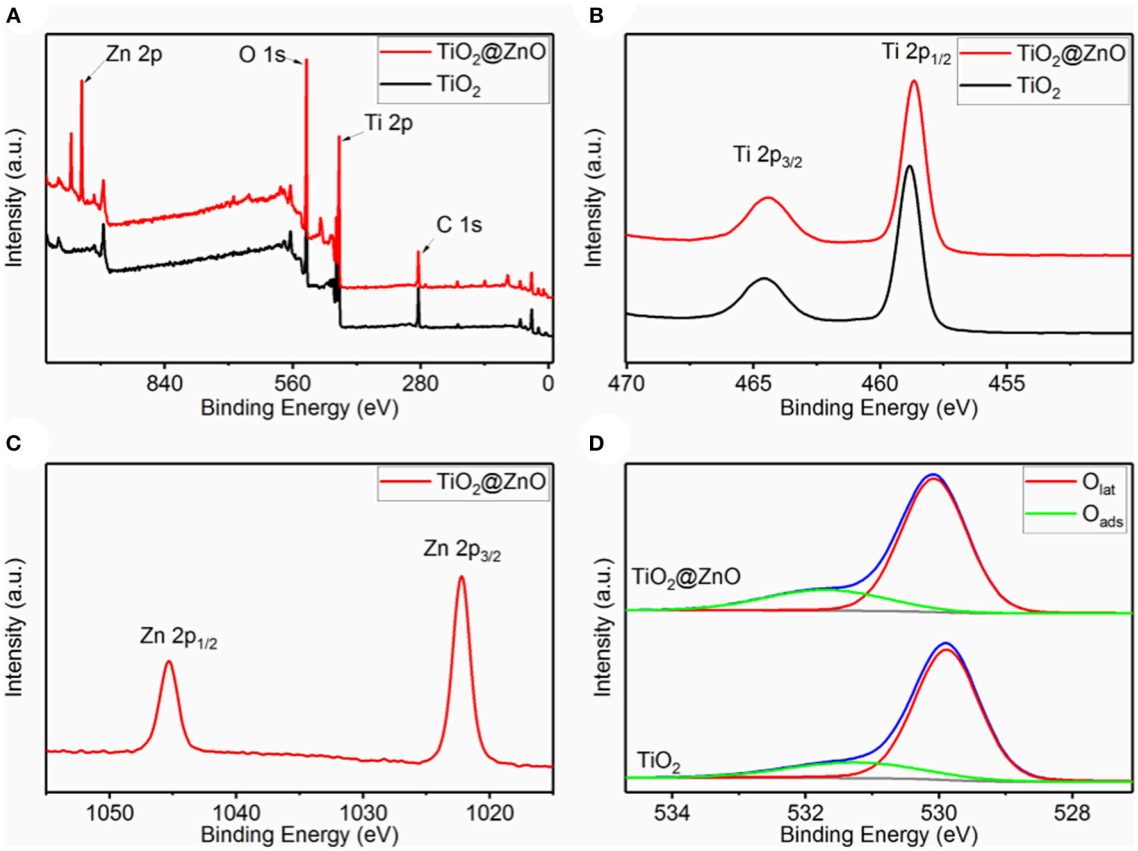

FIGURE 2 | X-ray photoelectron spectroscopy (XPS) spectra of pristine TiO_2 and TiO_2@ZnO nanotubes. **(A)** Survey spectrum, **(B)** Ti 2p, **(C)** Zn 2p, and **(D)** O 1s.

TiO_2 (19.5%), suggesting that ZnO decoration generated more surface adsorption sites.

Figures 3A–D show the SEM micrographs of the as-prepared ordered arrays of pristine TiO_2 and TiO_2@ZnO samples. The pore diameter of the pristine TiO_2 nanotubes is ∼80 nm with a wall thickness of ∼10 nm, and the length is ∼2.4 μm. There was no evident difference between the TiO_2@ZnO sample and the pristine one, indicating that the impregnation treatment did not affect the morphology of the nanotubes. EDS elemental mapping analysis was performed on TiO_2@ZnO as showed in **Figures 3E–G**, which revealed a homogeneous distribution of the Zn elements throughout the surface (**Figure 3G**). It can also be noticed that the Ti signal in the hollow part of the nanotube is more intense than that around the tube wall (**Figure 3F**), which can be ascribed to the unreacted Ti foil at the bottom. EDX analysis confirmed the coexistence of Ti, Zn, and O elements for the composite with a Zn/(Ti + Zn) ratio of 3.5 at%.

More in-depth microstructural analysis was performed on both samples with TEM (**Figure 4**). The pristine TiO_2 nanotubes presented a clear view (**Figure 4A**), while some extra nanoparticles in the size of 5–10 nm were observed with an even distribution throughout the ZnO-decorated nanotubes (**Figure 4B**). Selected area electron diffraction (SAED) revealed some extra diffraction pots in addition to the main diffraction rings of TiO_2 (**Figure 4C**), corresponding to the (100) and (002) planes of ZnO (JCPDS 36-4521). These results indicated that TiO_2 nanotubes modified with ZnO nanoparticles were successfully obtained.

Gas Sensing Properties

ZnO decoration was found to significantly increase the resistance in air of the TiO_2 nanotubes, corresponding to an increase in R_a from ∼40 kΩ to ∼6 MΩ at 300°C. **Figure 5A** compares the response of the sensors to 100 ppm H_2 at different temperatures. The pristine TiO_2 sensor exhibited typical volcano-shape temperature dependence of response. The response at the working temperature of 300°C is 126, which is 3.2 times that of samples with a tube length of 3–4 μm and a diameter of ∼100 nm under the same conditions (Xun et al., 2018). This indicates that the response can be increased by changing the morphology of nanotubes, i.e., reducing the diameter and length. A similar behavior of temperature dependence of response was observed, and the response was improved after the ZnO impregnation. At the optimum temperature of 350°C for both sensors, the response of the TiO_2@ZnO composite to 100 ppm H_2 was ∼520, about 1.8 times higher than that of pristine TiO_2.

Figure 5B shows that response increased with the increase in H_2 concentration for both kinds of sensors. A linear relationship between the response and H_2 concentration on the log–log scale was observed for all samples, which accords with the power–law theory proposed by Yamazoe and Shimanoe (2008). The response of the TiO_2@ZnO composite was higher than that of

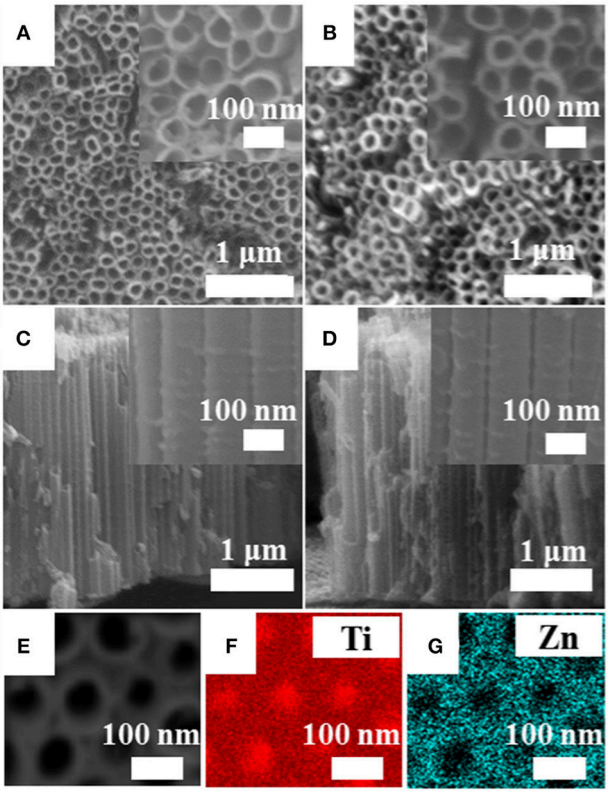

FIGURE 3 | Scanning electron microscopy (SEM) images of **(A,B)** surface and **(C,D)** cross-sectional view of **(A,C)** pristine TiO_2 and **(B,D)** TiO_2@ZnO nanotubes. Energy-dispersive spectrometer (EDS) elemental images of TiO_2@ZnO with **(E)** SEM images, **(F)** Ti, and **(G)** Zn.

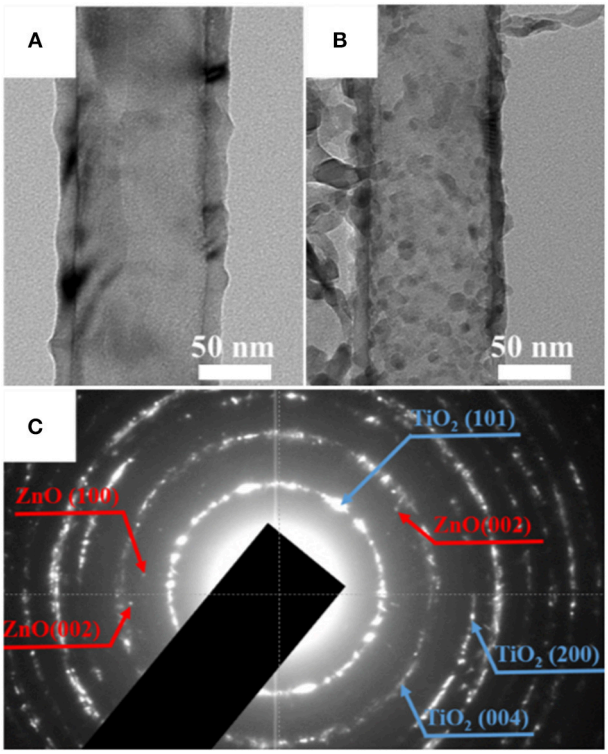

FIGURE 4 | Transmission electron microscopy (TEM) images of **(A)** pristine TiO_2 nanotubes and **(B)** TiO_2@ZnO composites. **(C)** SAED pattern of TiO_2@ZnO.

the pristine one at all tested concentrations, and the enhancement was more pronounced at higher concentrations. Taking $S = 1.2$ as the detection threshold (Liu et al., 2017; Gao et al., 2019), the detection limit calculated for the TiO_2@ZnO composite sensor was 7.5 ppm, which was smaller than that of the pristine TiO_2 sensor (10.3 ppm). It can also be seen that the response of two different TiO_2@ZnO sensors was very close to each other, indicating good consistency of the sensors.

Figure 5C shows that for both pristine TiO_2 and TiO_2@ZnO, the response time decreased as the concentration increased. A much faster response speed was observed for the latter sample. The response time of TiO_2@ZnO is 22 s for 100 ppm H_2 at 300°C, which is 4.2 times faster than that of the pristine sample. A power–law relationship was observed between the response time and the concentration, which may be accounted for by a nonlinear diffusion-reaction model (Xun et al., 2018). In contrast to the fast response speed, the recovery process was sluggish, typically with a recovery time over 2,000 s. Moreover, the recovery became slower while the concentration increased.

To illustrate the selectivity of the sensors, the response to 100-ppm various gases at 300°C was compared (**Figure 5D**). Because hydrogen is highly combustive and explosive, NH_3, C_3H_8, NO_2, CO, and CH_4 were selected to examine the cross-sensitivity, which are very common interfering gases for fire detection. It can be seen that the pristine TiO_2 showed some minor response to NH_3 and insignificant response to the other interfering gases. The response to both H_2 and NH_3 increased while that to other gases remained after ZnO decoration. Nevertheless, the H_2 response increased much more pronouncedly than the NH_3 one. As a result, the selectivity, i.e., the response ratio of H_2 over the most interfering gas, NH_3, increased from 19.6 to 82.3 after ZnO loading. It should be noted that humidity is also a very common interference for semiconductor gas sensors. Although the humidity effect was not tested for the present samples, a significant humidity effect has been observed for other similar gas sensors based on TiO_2 nanotubes in our group's research. Some strategies have been adopted to eliminate the humidity impact, e.g., by using a reference element for compensation (Zhan et al., 2007) or by decorating hydrophobic materials (Yao et al., 2016).

Gas Sensing Mechanism

The relatively high sensitivity of pristine TiO_2 toward H_2 can be attributed to the unique hierarchical morphology of the nanotubes. The small half-tube-wall thickness is comparable to that of the space charge layer, which favors hydrogen adsorption and its reaction with surface oxygen (Paulose et al., 2005; Hazra et al., 2015). The improved H_2 response of TiO_2@ZnO may be a result of the synergistic contribution from two effects. Firstly, the enhanced O_2 adsorption due to ZnO decoration

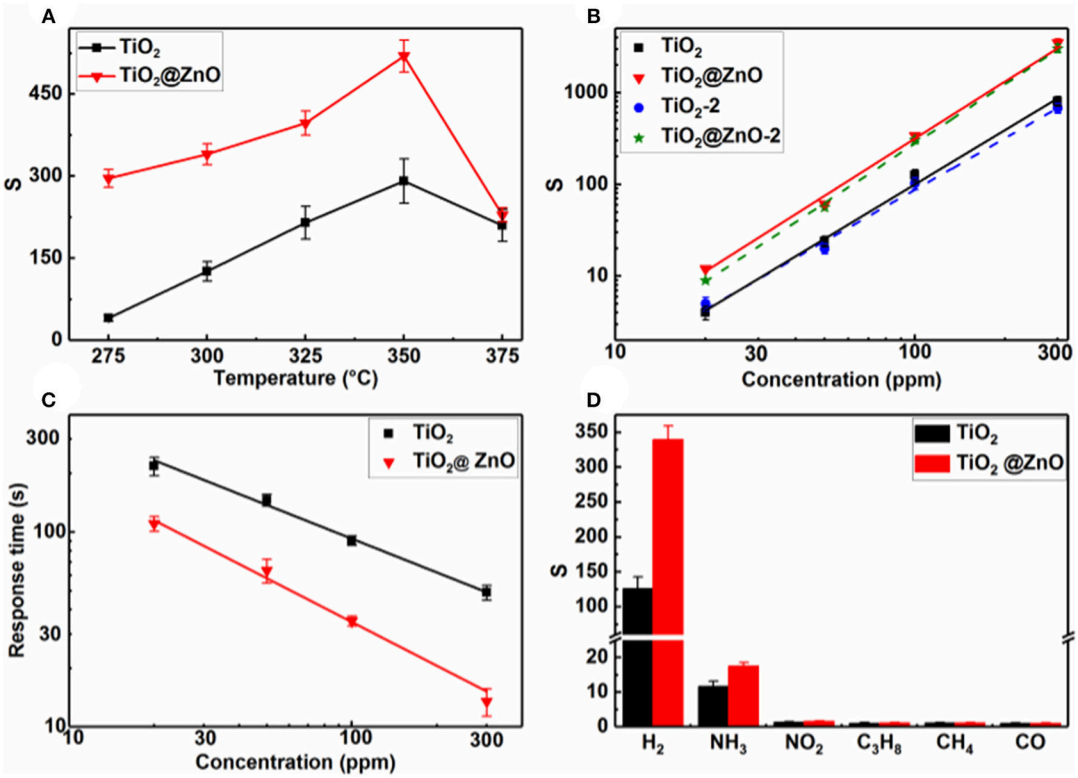

FIGURE 5 | Response of pristine TiO_2 and TiO_2@ZnO composite sensors as a function of **(A)** temperature to 100-ppm H_2 and **(B)** H_2 concentration at 300°C; **(C)** response time of pristine TiO_2 and TiO_2@ZnO composite sensors vs. H_2 concentration at 300°C; **(D)** response of pristine TiO_2 and TiO_2@ZnO composite sensors to 100-ppm various gases at 300°C.

revealed by XPS in **Figure 2** suggested generation of more active sites on the material surface, which is beneficial to the gas surface reactions. Secondly, n-n heterojunctions would be formed between the ZnO nanoparticles and TiO_2 nanotubes. Previous research has reported that ZnO (3.37 eV) has a slightly larger band gap than that of TiO_2 (3.2 eV); (Lin et al., 2013), and both conduction band energy and valance band energy of ZnO are higher than those of TiO_2, leading to transfer of electrons from the conduction band of ZnO to that of TiO_2 (Yang et al., 2009; Sarkar et al., 2014; Ng et al., 2018). Heterojunctions formed on the materials surface have been suggested to benefit the gas sensing performance *via* several routes, such as promoting gas reactions and regulating the conduction channel inside the materials (Lou et al., 2013; Li et al., 2015b; Gu et al., 2017), which can be applied to explain the enhancement of the composite sensor in this work.

CONCLUSIONS

Highly ordered TiO_2 nanotube arrays were synthesized by anodic oxidation. Decoration of ZnO nanoparticles on the nanotubes was achieved by immersion and calcination. Gas sensing test results indicate that significantly larger response and better selectivity to H_2 as well as shorter response time were achieved by ZnO loading. The TiO_2@ZnO sensor exhibited a response as high as 520 toward 100-ppm H_2 at 350°C. The excellent gas sensing performance of the composite may be attributed mainly to the highly ordered nanotube morphology and heterojunction formation at the interface of ZnO and TiO_2.

AUTHOR CONTRIBUTIONS

JY designed the experiments. AY and HX conducted the experiments and analyzed the results. JY and AY wrote the manuscript.

FUNDING

This work was supported by the National Natural Science Foundation of China (grant nos. 61871359 and U1432108).

REFERENCES

Chen, D., and Yi, J. (2018). One-pot electrospinning and gas-sensing properties of $LaMnO_3$ perovskite/SnO_2 heterojunction nanofibers. *J. Nanopart. Res.* 20:65. doi: 10.1007/s11051-018-4158-x

Gao, H., Yu, Q., Chen, K., Sun, P., Liu, F., Yan, X., et al. (2019). Ultrasensitive gas sensor based on hollow tungsten trioxide–nickel oxide (WO_3-NiO) nanoflowers for fast and selective xylene detection. *J. Colloid Interface Sci.* 535, 458–468. doi: 10.1016/j.jcis.2018.10.010

Gu, D., Li, X., Zhao, Y., and Wang, J. (2017). Enhanced NO_2 sensing of SnO_2/SnS_2 heterojunction based sensor. *Sens. Actuators B* 244, 67–76. doi: 10.1016/j.snb.2016.12.125

Hazra, A., Bhowmik, B., Dutta, K., Chattopadhyay, P., and Bhattacharyya, P. (2015). Stoichiometry, length, and wall thickness optimization of TiO_2 nanotube array for efficient alcohol sensing. *ACS Appl. Mater. Interfaces* 7, 9336–9348. doi: 10.1021/acsami.5b01785

Hübert, T., Boon-Brett, L., Black, G., and Banach, U. (2011). Hydrogen sensors—a review. *Sens. Actuators B* 157, 329–352. doi: 10.1016/j.snb.2011.04.070

Joo, S., Muto, I., and Hara, N. (2010). Hydrogen gas sensor using Pt-and Pd-added anodic TiO_2 nanotube films. *J. Electrochem. Soc.* 157, J221–J226. doi: 10.1149/1.3374643

Li, T., Zeng, W., and Wang, Z. (2015a). Quasi-one-dimensional metal-oxide-based heterostructural gas-sensing materials: a review. *Sens. Actuators B* 221, 1570–1585. doi: 10.1016/j.snb.2015.08.003

Li, W., Ma, S., Li, Y., Yang, G., Mao, Y., Luo, J., et al. (2015b). Enhanced ethanol sensing performance of hollow ZnO–SnO_2 core–shell nanofibers. *Sens. Actuators B* 211, 392–402. doi: 10.1016/j.snb.2015.01.090

Lin, L., Yang, Y., Men, L., Wang, X., He, D., Chai, Y., et al. (2013). A highly efficient TiO_2@ ZnO n–p–n heterojunction nanorod photocatalyst. *Nanoscale* 5, 588–593. doi: 10.1039/c2nr33109h

Liu, J., Wang, T., Wang, B., Sun, P., Yang, Q., Liang, X., et al. (2017). Highly sensitive and low detection limit of ethanol gas sensor based on hollow ZnO/SnO_2 spheres composite material. *Sens. Actuators B* 245, 551–559. doi: 10.1016/j.snb.2017.01.148

Lou, Z., Li, F., Deng, J., Wang, L., and Zhang, T. (2013). Branch-like hierarchical heterostructure (α-Fe_2O_3/TiO_2): a novel sensing material for trimethylamine gas sensor. *ACS Appl. Mater. Interfaces* 5, 12310–12316. doi: 10.1021/am402532v

Miller, D. R., Akbar, S. A., and Morris, P. A. (2014). Nanoscale metal oxide-based heterojunctions for gas sensing: a review. *Sens. Actuators B* 204, 250–272. doi: 10.1016/j.snb.2014.07.074

Mor, G. K., Varghese, O. K., Paulose, M., Shankar, K., and Grimes, C. A. (2006). A review on highly ordered, vertically oriented TiO_2 nanotube arrays: Fabrication, material properties, and solar energy applications. *Sol. Energy Mater. Sol. Cells* 90, 2011–2075. doi: 10.1016/j.solmat.2006.04.007

Ng, S., Kuberský, P., Krbal, M., Prikryl, J., Gärtnerová, V., Moravcová, D., et al. (2018). ZnO coated anodic 1D TiO_2 nanotube layers: efficient photo-electrochemical and gas sensing heterojunction. *Adv. Eng. Mater.* 20:1700589. doi: 10.1002/adem.201700589

Paulose, M., Varghese, O. K., Mor, G. K., Grimes, C. A., and Ong, K. G. (2005). Unprecedented ultra-high hydrogen gas sensitivity in undoped titania nanotubes. *Nanotechnology* 17:398. doi: 10.1088/0957-4484/17/2/009

Sarkar, A., Singh, A. K., Khan, G. G., Sarkar, D., and Mandal, K. (2014). TiO_2/ZnO core/shell nano-heterostructure arrays as photo-electrodes with enhanced visible light photoelectrochemical performance. *RSC Adv.* 4, 55629–55634. doi: 10.1039/c4ra09456e

Şennik, E., Colak, Z., Kılınç, N., and Ozturk, Z. Z. (2010). Synthesis of highly-ordered TiO_2 nanotubes for a hydrogen sensor. *Int. J. Hydrogen Energy* 35, 4420–4427. doi: 10.1016/j.ijhydene.2010.01.100

Silva, S. F., Coelho, L., Frazão, O., Santos, J. L., and Malcata, F. X. (2012). A review of palladium-based fiber-optic sensors for molecular hydrogen detection. *IEEE Sens. J.* 12, 93–102. doi: 10.1109/jsen.2011.2138130

Varghese, O. K., Gong, D., Paulose, M., Ong, K. G., and Grimes, C. A. (2003). Hydrogen sensing using titania nanotubes. *Sens. Actuators B* 93, 338–344. doi: 10.1016/s0925-4005(03)00222-3

Wang, Y., Wu, T., Zhou, Y., Meng, C., Zhu, W., and Liu, L. (2017). TiO_2-based nanoheterostructures for promoting gas sensitivity performance: designs, developments, and prospects. *Sensors* 17:1971. doi: 10.3390/s17091971

Xiong, Y., Chen, W., Li, Y., Cui, P., Guo, S., Chen, W., et al. (2016). Contrasting room-temperature hydrogen sensing capabilities of Pt-SnO_2 and Pt-TiO_2 composite nanoceramics. *Nano Res.* 9, 3528–3535. doi: 10.1007/s12274-016-1229-0

Xun, H., Zhang, Z., Yu, A., and Yi, J. (2018). Remarkably enhanced hydrogen sensing of highly-ordered SnO_2-decorated TiO_2 nanotubes. *Sens. Actuators B* 273, 983–990. doi: 10.1016/j.snb.2018.06.120

Yamazoe, N., and Shimanoe, K. (2008). Theory of power laws for semiconductor gas sensors. *Sens. Actuators B* 128, 566–573. doi: 10.1016/j.snb.2007.07.036

Yang, H. Y., Yu, S. F., Lau, S. P., Zhang, X., Sun, D. D., and Jun, G. (2009). Direct growth of ZnO nanocrystals onto the surface of porous TiO_2 nanotube arrays for highly efficient and recyclable photocatalysts. *Small* 5, 2260–2264. doi: 10.1002/smll.200900724

Yao, M. S., Tang, W. X., Wang, G. E., Nath, B., and Xu, G. (2016). MOF thin film-coated metal oxide nanowire array: significantly improved chemiresistor sensor performance. *Adv. Mater.* 28, 5229–5234. doi: 10.1002/adma.201506457

Zhan, Z., Lu, J., Song, W., Jiang, D., and Xu, J. (2007). Highly selective ethanol In_2O_3-based gas sensor. *Mater. Res. Bull.* 42, 228–235. doi: 10.1016/j.materresbull.2006.06.006

Zhang, J., Liu, X., Neri, G., and Pinna, N. (2016). Nanostructured materials for room-temperature gas sensors. *Adv. Mater.* 28, 795–831. doi: 10.1002/adma.201503825

Zhao, Z., Tian, J., Sang, Y., Cabot, A., and Liu, H. (2015). Structure, synthesis, and applications of TiO_2 nanobelts. *Adv. Mater.* 27, 2557–2582. doi: 10.1002/adma.201405589

Conflict of Interest Statement: The authors declare that the research was conducted in the absence of any commercial or financial relationships that could be construed as a potential conflict of interest.